Gamow-Teller and first-forbidden decays near the *r*-process paths at $N=50$, 82, and 126

I. N. Borzov*
Institute for Nuclear Theory, University of Washington, Box 351550, Seattle, Washington 98195
and Institut d'Astronomie et d'Astrophysique, Universite Libre de Bruxelles, CP226, Bvd. duTriomphe, 1050 Bruxelles, Belgium
(Received 26 September 2002; published 27 February 2003)

The β-decay rates of neutron-rich nuclei relevant to the *r*-process nucleosynthesis are mostly beyond experimental reach. Their predictions demand a self-consistent extrapolation of various nuclear properties away from the experimentally known regions. The allowed transitions approximation commonly used in large-scale microscopic calculations also needs to be revised in different mass regions. The density functional+continuum QRPA approximation to self-consistent calculations of the ground state properties, Gamow-Teller and first-forbidden β-decay transitions of nuclei far from stability is developed. Systematic calculations are performed of the allowed and first-forbidden β-decay rates for the *r*-process relevant nuclides near the closed neutron shells at $N=50,82,126$. The importance of first-forbidden decays near $Z\geqslant 50$, $N\approx 82$ and near $N=126$ is shown. The total β-decay half-lives in the region ''east'' of the ^{208}Pb are estimated. A comparison with recent experimental data, global calculations, and self-consistent microscopic predictions is presented.

DOI: 10.1103/PhysRevC.67.025802 PACS number(s): 23.40.Bw, 21.60.Jz, 25.30.Pt, 26.30.+k

I. INTRODUCTION

The various supernova models fail so far in predicting the physical conditions necessary for a successful *r*-process nucleosynthesis [1]. In addition to numerous problems in the quest of the astrophysical site for the *r* process, nuclear physics uncertainties are still high. To describe the production of the *r*-process isotopes, the knowledge of the properties of thousands of (mostly unknown) neutron-rich nuclei is required. Those include the characteristics of strong, electromagnetic and weak interaction processes. In particular, β^- decays play a key role since they are the major mechanism for driving the material to heavier elements and for setting the *r*-process time scale. In the case where the *r* process takes place in a neutrino-rich environment, charged-current electron neutrino captures, could amplify the effect of the β decays. It could also change the *r*-abundance distribution by subsequent ν-induced neutron spallation [2]. Hence, it is of great importance to make reliable predictions of nuclear weak interaction rates for very neutron-rich nuclei.

The nuclear models fitted to experimental data close to the β-stability line usually allow for a crude extrapolation to extreme isospin values. For the *r*-process calculations, self-consistent models are mandatory. The predictions of the β-decay rates based on the same ground state description, as the one used to calculate the nuclear masses provide more reliable extrapolation far from stability. This is essential in order to ensure the internal consistency of the nucleosynthesis models.

Two different microscopic approaches have been used in the large-scale calculation of weak rates for *r*-process applications—the shell-model and the quasiparticle random-phase approximation (QRPA). The advantage of the shell model is the possibility to take into account the detailed structure of the β-strength functions. It has been applied to calculate the Gamow-Teller (GT) β-decay rates for a number of the *r*-process relevant neutron-rich nuclides at $N=50,82$ [3] and also at $N=126$ [4]. The ''no-core'' calculations using the effective interactions and multi-$\hbar\Omega$ model space are feasible for the GT decay of light nuclei [5]. For heavier nuclei, a truncation of the basis is inevitable even for the GT decay. As different oscillator shells are involved for the first-forbidden decays, a multi-$\hbar\Omega$ treatment is needed in this case. A ''valence-core'' calculations of the forbidden decays in the tin and lead region were done in Ref. [6]. The shell model with continuum has been applied to forbidden decay of light nuclei [7]. The density matrix renormalization group method [8] can be used in large-scale shell-model calculations. The problem of self-consistency of the multi-$\hbar\Omega$ shell-model calculations has been discussed in Ref. [9].

The up-to-date QRPA approach is based on the self-consistent predictions for the ground state within the continuum HFB [10]. The excited states can be treated in a linear response theory with exact account for the whole continuum (unrestricted ph configuration space) [11,12]. For the ground state pairing, well defined basis regularization schemes exist [10,13]. The QRPA models used for large-scale calculations of the β rates have considered so far simple particle-hole (ph) configurations, but this limitation is not a principal one and can be removed.

The first QRPA models for the $\beta^{\pm}$-decay half-lives which replaced the phenomenological ''gross theory'' [14] lacked self-consistency and relied on separable effective NN interactions. They were based on the Nilsson+BCS formalism [15] or on the finite-range droplet model with a folded Yukawa single-particle potential (FRDM+QRPA) [16]. The scheme of Ref. [15] was extended to unique first forbidden transitions, but this decay channel is important in special cases only.

The first self-consistent HF-BCS+continuum QRPA (CQRPA) model for the β-decay half-lives has been developed in Ref. [17] within the finite Fermi system theory (FFS) [18]. The self-consistent ETFSI+CQRPA approximation to the ground state masses and weak processes rates has been

*Also at State Scientific Centre–Institute of Physics and Power Engineering, 249020 Obninsk, Russia.

elaborated in Ref. [19]. It was used in the coherent large-scale predictions of nuclear masses, β^--decay rates, and ν_e-capture rates in Ref. [20], as well as of $\bar{\nu}_e$-capture rates [21]. The self-consistent treatment of the ground state properties and consideration of the particle-particle (pp) effective interaction resulted in a more realistic evaluation of odd-even effects in the total half-lives [17,19,20] compared to the FRDM tables [16]. The β^--decay rates of spherical even-even semimagic nuclides with $N=50$, 82, and 126 have been calculated within the HFB+QRPA with a Skyrme energy-density functional in Ref. [22]. The results are close to those of Ref. [20] provided the same effective p-interaction is adopted. The first-forbidden decays for the r-process relevant nuclides at $N=50,82$ have been treated recently within the self-consistent HF-BCS+CQRPA in Ref. [23].

Experiments using a new generation of the radioactive ion beam facilities are crucial in validation of the theories. Great attention has been paid to the nuclei near the closed neutron shells at $N=50$, 82, and 126 of special importance for the r-process modeling. The high precision data for short-lived Ni isotopes near ^{78}Ni [24], $^{121-129}$Ag isotopes, [25] and $^{133-137}$Sn [26] have been measured at RILIS (CERN), which benefits from the high isotopic and isobaric selectivity reached by a laser ion source and by mass spectroscopy, respectively. The current experimental studies in the neutron-rich and neutron-deficient lead regions [27,28] are very important for studying the evolution of nuclear structure at extreme isospin, as well as for elucidating the weak interaction and β-decay theories.

A detailed theoretical study of the β decays near the closed shells at $N=50$, 82, and 126 is of key importance. It provides a clear case for application of the CQRPA model, for a comparison of different methods and for experimental check. First, these nuclei are not extreme drip-line systems ($S_n \approx 2.0-3.0$ MeV$>\Delta$, where Δ is the pairing potential), therefore a mean-field approach is relevant. Second, most of these nuclei are spherical, hence their β-decay half-lives are very sensitive to nuclear structure effects. Third, the nuclei with $Z\approx 28$ near ^{78}Ni and $Z\approx 50$ near ^{132}Sn undergo high-energy GT and/or first-forbidden β decays. In these conditions, the spherical, $1p1h$-QRPA approaches accounting for the allowed and first-forbidden transitions have a reasonable accuracy in predicting the β-decay half-lives.

Up to now, there have been no microscopic large-scale calculations performed beyond the allowed β-decay approximation, which certainly needs to be revised in different mass regions. It has been argued that the relative contribution of the GT and first-forbidden β decays may vary in the vicinity of the $Z\geqslant 50$ nuclei near $N=82$ and for the nuclei near $N=126$ [20,23]. It is of prime interest to perform systematic calculations for those heavy r-process relevant nuclei where the first-forbidden transitions are expected to play an important role.

The outline of the paper is as follows. In Sec. I the developed density functional+CQRPA approximation is described in detail. It is shown that the method is appropriate for self-consistent large-scale calculations of the ground state properties, Gamow-Teller and first-forbidden β-decay rates of heavy nuclei far from the β-stability line. In Sec. II the results of systematic calculations are presented for the allowed and first-forbidden β-decay rates near the closed neutron shells at $N=50,82,126$.

II. THEORETICAL FRAMEWORK

In the normal approximation $pR\ll 1$, $qR\ll 1$, the electron (p) and neutrino (q) momenta are smaller than the momentum of order of $1/R$ transferred to nucleus (here $R=r_0A^{1/3}$ is the nuclear radius). The allowed GT and first-forbidden decays from the parent nucleus ground state $|i\rangle$ to the final states $|f\rangle$ of the daughter nucleus depend on seven β moments related to the nuclear matrix elements of the following operators:

$$\vec{\sigma},$$

$$\gamma_5,[\vec{\sigma}\vec{r}]^{(0)},$$

$$\alpha,\vec{r},[\vec{\sigma}\vec{r}]^{(1)},$$

$$[\vec{\sigma}\vec{r}]^{(2)},$$

where $\vec{\sigma}$ are the Pauli spin matrices and the rank of the tensor operators $[\vec{\sigma}\vec{r}]^{(J)}$ is defined by the momentum $|J_i-J_f|\leqslant J\leqslant|J_i+J_f|$ transferred to the daughter nucleus. Allowed and unique transitions involve only single β moments, while the β rates of the nonunique decays are determined by incoherent (and mutually cancelling) contribution of different β moments. In addition, for $J=0,1$ transitions, the relativistic vector operator α and axial charge operator γ_5 should be included alongside with the spacelike operators. In a nonrelativistic limit the former corresponds to the velocity-dependent fields $\vec{P}/2M$ and $\vec{\sigma}\cdot\vec{P}/2M$, where $P=P_i+P_f$ is the total momentum transferred to the nucleus and M is the bare nucleon mass. Thus, the consistent treatment of the medium induced fields requires to take into account the velocity-dependent and two-body spin-orbit effective NN interactions. This complicates the large-scale calculations substantially.

The present model for large-scale calculations of the total half-lives of the first-forbidden decays is based on the self-consistent description of the ground states within the density functional approach. To find the mean field and pairing potentials, and a quasiparticle basis with account for the pairing correlations, we use the Fayans phenomenological density functional [10]. The dependence on the normal density ρ is simulated by fractional-linear functions and the surface energy is related to the density-dependent finite-range forces. The quasiparticle spectrum and wave functions are calculated from a self-consistent mean field which is the first functional derivative of the interaction energy with respect to the normal density, while the pairing potential is obtained as the functional derivative of the pairing energy with respect to the anomalous nucleon density ν. An additional self-consistency condition [29] is used which removes a spurious isospin mixing for Fermi (F) transitions.

The excited states are treated within the continuum QRPA-like framework of the finite Fermi system (FFS) theory [18] with exact treatment of the particle-hole (ph) continuum, density-dependent pairing and finite-range effective NN interactions in the particle-hole and particle-particle (pp) channels. The perturbation theory can be used in order to simplify the treatment of the velocity dependent nuclear responses. However, for global calculations of the total half-lives, it is convenient to replace them by the space-dependent fields. The exact nonrelativistic relation between the matrix elements of the timelike operator α and its spacelike counterpart $\vec{r}$ can be applied which reflects the conservation of the nuclear vector current (CVC) [30]. For the timelike operator γ_5 and its spacelike counterpart $\vec{\sigma}\cdot\vec{r}$, no analogous exact relation exist due to the partial conservation of the axial current (PCAC). The self-consistent FFS sum rule approach [31] helps to approximate the operator γ_5 by the spacelike operator $\vec{\sigma}\cdot\vec{r}$ taking into account the medium corrections. With the resulting set of the space-dependent external fields the large-scale calculations of the β-decay half-lives are feasible.

A. The ground-state description

The total interaction energy of a superfluid nucleus $E_{\rm int}[\rho,\nu]=\int d\vec{r}\ \varepsilon_{\rm int}(\vec{r};[\rho,\nu])$, is a functional of two densities, the normal one $\rho(\vec{r})$, and the anomalous one $\nu(\vec{r})$. Self-consistent calculations with such a functional look similar to the standard variational HFB procedure in which the single-particle Hamiltonian takes the form

$$\mathcal{H}=\begin{pmatrix} h-\mu & \Delta \\ -\Delta^* & \mu-h \end{pmatrix}, \tag{1}$$

where

$$h=\frac{p^2}{2M}+\frac{\delta E_{\rm int}[\rho,\nu]}{\delta\rho}, \quad \Delta=-\frac{\delta E_{\rm int}[\rho,\nu]}{\delta\nu}. \tag{2}$$

The Hamiltonian h contains the free kinetic energy operator (the quasiparticle effective mass m^* being equal to the bare nucleon mass M). The interaction energy density is written as

$$\varepsilon_{\rm int}=\varepsilon_{\rm main}+\varepsilon_{\rm Coul}+\varepsilon_{sl}+\varepsilon_{\rm pair}, \tag{3}$$

where $\varepsilon_{\rm main}$ contains the volume isoscalar and isovector contributions, and also the surface isoscalar and isovector interaction energies generated by the density-dependent finite-range forces (see Ref. [10], and references therein). The Coulomb interaction energy density $\varepsilon_{\rm Coul}$ takes its usual form and includes the exchange part in the Slater approximation. The spin-orbit self-consistent potential ε_{sl} in Eq. (3) comes from the two-body spin-orbit effective NN interaction

$$F_{sl}^{\tau\tau'}=4N_0^{-1}r_{sl}^2\kappa^{\tau\tau'}[\vec{\nabla}_1\delta(\vec{r}_1-\vec{r}_2)\times(\vec{p}_1-\vec{p}_2)]\cdot(\vec{\sigma}_1+\vec{\sigma}_2), \tag{4}$$

and from the first-order velocity harmonic of the spin-dependent Landau-Migdal effective NN interactions

$$F_{(\sigma p)}=4N_0^{-1}r_{sl}^2(g_1+g_1'\vec{\tau}_1\cdot\vec{\tau}_2)\,\delta(\vec{r}_1-\vec{r}_2)(\vec{\sigma}_1\cdot\vec{\sigma}_2)(\vec{p}_1\cdot\vec{p}_2). \tag{5}$$

Here the operators $\vec{p}_{1,2}$ do not act on the $\delta(\vec{r}_1-\vec{r}_2)$. Thus, the spin-orbit effective interaction generates the single-particle potential consisting of the usual term and central component

$$\hat{U}_{sl}=U_{sl}^{\tau}(\vec{r})\vec{\sigma}\vec{l}+U_{sl-o}^{\tau}(r) =4N_0^{-1}r_0^2\sum_{\tau'}\kappa^{\tau\tau'}\left[\frac{1}{r}\frac{d\rho^{\tau'}}{dr}\vec{\sigma}\cdot\vec{l}-\frac{1}{r^2}\frac{d}{dr}(\rho_{sl}^{\tau'}r)\right]. \tag{6}$$

The spin-orbit density is given by

$$\rho_{sl}^{\tau}=\sum_{\lambda}\ n_{\lambda}^{\tau}\langle\vec{\sigma}\cdot\vec{l}\rangle_{\lambda}|\phi_{\lambda}^{\tau}(\vec{r})|^2, \tag{7}$$

here N_0^{-1} is inverse density of states at the Fermi surface defined as $2N_0^{-1}=C_0=300$ MeV fm^3, with $C_0=2\varepsilon_F/3\rho_0$, and $\rho_0=0.0859$ fm^{-3} being the equilibrium density of one kind of particles in the symmetric nuclear matter, $r_{sl}=(3/8\pi\rho_0)^{2/3}$ is a dimensionality factor, $\kappa^{\tau\tau'}=(\kappa^{+}+\kappa^{-}\vec{\tau}_1\cdot\vec{\tau}_2)$ and g_1, g_1' are the dimensionless FFS constants, $n_{\lambda}^{\tau}=v_{\lambda,\tau}^2$ are the occupancy factors of the quasiparticle levels λ^{τ}, ϕ_{λ}^{τ} are their wave functions ($\lambda^{\tau}=nlj\mu\tau$ is the standard set of the quantum numbers, $\tau=n,p$), and $\langle\vec{\sigma}\cdot\vec{l}\rangle_{\lambda}=j(j+1)-l(l+1)-3/4$.

The fully self-consistent approach should include these velocity dependent effective interactions both for the ground and excited states calculations. Thus, the effective NN-interaction should contain non-local terms in the scattering channel which complicates the QRPA problem. In order to facilitate the large-scale calculations, the velocity-dependent interactions are not included in the present model at the QRPA level. At the ground state level, an additional self-consistency condition is applied which is associated with a spontaneous breaking of the isospin symmetry. It relates the symmetry potential to the charge-exchange density-dependent effective NN interaction $F_{\tau}^{-}=F^{nn}-F^{np}=F^{pp}-F^{np}$:

$$F_{\tau}^{-}=4N_0^{-1}\left[a_{\delta}'\delta(\vec{r}_{12})+a_r'u(\vec{r}_{12})+\frac{b}{4\rho_0}\rho^{+}\left(\frac{\vec{r}_1+\vec{r}_2}{2}\right)\delta(\vec{r}_{12})\right]. \tag{8}$$

The strength parameters a_{δ}', a_r' and b [31] are related to the usual FFS parameters as follows: $f_{\rm in}'=a_{\delta}'+a_r'-b/2$ and $f_{\rm ex}'=a_{\delta}'+a_r'$, where $f_{\rm in}'(f_{\rm ex}')$ are the isovector interaction strengths inside (outside) the nucleus, $u(r)$ is the normalized Yukawa function, $\rho^{+}=\rho^{n}+\rho^{p}$ is the isoscalar density. These parameters may be constrained from the additional self-consistency condition [29]

$$U^-(\vec{r}) = (F_\tau^-(\vec{r},\vec{r}';[\rho])\rho^-(\vec{r}')), \tag{9}$$

where $U^-(\vec{r}) = U^n(\vec{r}) - U^p(\vec{r})$ and $\rho^-(\vec{r}) = \rho^n(\vec{r}) - \rho^p(\vec{r})$. Here, and below, each pair of external brackets indicates the integration on the spatial coordinates.Within the full basis CQRPA, the relation Eq. (9) excludes the spurious isospin mixing for the Fermi transitions. It is more convenient to use an integral analog of Eq. (9) relating the double-folded monopole component of F_τ^- to the potential symmetry energy $E_s = \beta_s(N-Z)^2/A$

$$E_s \equiv 2\pi(U^-(r)\rho^-(r)) = 2\pi((\rho(r)F_0^-(r,r';[\rho])\rho(r'))). \tag{10}$$

The second term in Eq. (3) is the pairing energy density $\varepsilon_{\rm pair} = \frac{1}{2}\nu^\dagger F^\xi \nu$, where the effective force in the particle-particle channel is

$$F^\xi(\vec{r}_{12}) = -4N_0^{-1} f^\xi(x)\,\delta(\vec{r}_{12}). \tag{11}$$

The $f^\xi(x)$ is a dimensionless strength treated in the local density approximation as a (local) functional of the isoscalar density $x = (\rho_p + \rho_n)/2\rho_0$, the $\rho_{p,(n)}$ are the proton (neutron) densities. This is expressed in a Skyrme-like form [10]

$$f^\xi(x) = f_{\rm ex}^\xi + h^\xi x^q(\vec{r}), \tag{12}$$

where $f_{\rm ex}^\xi$ is negative (attractive in the pp channel), $h^\xi x^q(\vec{r})$ is positive with $q = 2/3$ (a repulsive short-range part), the gradient term is omitted. The superscript ξ refers to the energy cutoff parameter. It defines the number of single-particle levels taken into account when evaluating the anomalous Green's functions and, correspondingly, when solving the equations for the pairing fields $\Delta(\vec{r})$ and chemical potentials μ, as well as the QRPA equations for the excited states. In the case of the density dependent pairing, a local cutoff treatment of the pairing energy density [10] helps to avoid the problem of the cutoff energy. An efficient pairing regularization procedure has been suggested in Ref. [13].

The pairing has been treated in the diagonal approximation. For the contact pairing force, this corresponds to the self-consistent HF-BCS calculations. In the case of the density independent pairing, the strength parameter in Eq. (12) is chosen to reproduce the empirical matrix elements of the pairing potential Δ^τ. It varies in the range of $f^\xi = 0.25$–0.33 (in units of $4N_0^{-1}$), depending on the mass number if the pp basis includes all the single-particle states with energies less than $E_{\rm cutoff} = 15$ MeV. For the density dependent pairing option the use is made of $f_{\rm ex}^\xi = -0.89$, $h^\xi = 0.83$ with the $E_{\rm cutoff} = 40$ MeV [10].

In the present work, the parameter set DF3 [17] of the Fayans density functional is used. It reproduces not only the known ground-state properties of (magic) nuclei but also the single-particle energies near the ''magic cross'' at ^{132}Sn [32]. The β-decay calculations have also been performed with the ground state description given by the (MSk7) Skyrme type density functional [33]. The corresponding Skyrme force contains ten parameters, a δ-function pairing force with four parameters plus a A-dependent cutoff. The important difference with the DF3 is that the parameters of Msk7 (including the pairing strengths) are subject to the additional constraint of fitting at best the measured masses. The root-mean-square error of the fit to the 1888 measured masses given in Ref. [34] is 738 keV. As the pairing parameters are treated as free parameters in such a fitting, the balance of the mean vs pairing fields given by the self-consistent HF-BCS might be destroyed. One of the aims of the present work is to study whether the Msk7 parameters found in such a way allow, at the same time, a reasonable description of the basic nuclear properties (such as single-particle energies, etc.) crucial for the β-decay rates predictions.

It is of interest to note that, so far, the large-scale calculations of the masses [10,33,35] and the self-consistent predictions of the β-decay half-lives [17,20,22,23] have used phenomenological density functionals or energy-independent effective NN interactions. One of the alternatives is to construct the energy-dependent effective NN-interaction from the vacuum NN-scattering amplitude. Recently, such a calculation of the ground-state masses has been performed within the so-called quasiparticle Lagrange version of the self-consistent FFS [36]. It has been shown that for small values of the neutron chemical potential, the parameters of the effective NN interaction, and consequently the self-consistent mean fields, vary strongly. As the result, the neutron drip-line position shifts to very large values of the neutron excesses [36]. Such a modification of the ground state characteristics for neutron-rich nuclei may, for instance, change the concentration of the r-process ''seed'' nuclei.

B. Spin-isospin charge-exchange effective NN interaction

The spin-isospin effective NN interaction in the particle-hole (ph) channel written in the transferred momenta ($\vec{k}$) space is

$$F_{\sigma\tau}^\omega = 4N_0^{-1}\left[g_0'\vec{\sigma}_1\cdot\vec{\sigma}_2 + g_\pi e_{q\pi}^2 \frac{(\vec{\sigma}_1\cdot\vec{k})(\vec{\sigma}_2\cdot\vec{k})}{k^2+m_\pi^2+P_\Delta(k^2)} + g_\varrho e_{q\rho}^2 \frac{[\vec{\sigma}_1\vec{k}][\vec{\sigma}_2\vec{k}]}{k^2+m_\varrho^2}\right]\tau_1\cdot\tau_2. \tag{13}$$

Here $g_\pi = -2\pi/N_0\ (f_\pi^2/m_\pi^2)$, $g_\varrho = -2\pi/N_0\ (f_\varrho^2/m_\varrho^2)$, where $m_\pi(m_\varrho)$ and $f_\pi(f_\varrho)$ are the bare pion (ϱ-meson) mass and the $\pi NN(\varrho NN)$ coupling constants, respectively. The pion irreducible polarization operator in the nuclear medium $P_\Delta(k^2)$ takes care of the virtual Δ isobar-nucleon hole excitations. The contact part of the effective spin-isospin interaction Eq. (14) is governed by the Landau-Migdal constant g_0'. The operator $e_{q\pi}^2 = Q = e_q[\sigma\tau]^2$ is assumed to describe the quenching of the pion-nucleon vertex [18]. The operator $e_{q\varrho}^2$ is defined from the condition that the ϱNN coupling strength is $g_\varrho = 0.4 g_\varrho^{\rm bare}$ due to the short-range NN correlations.

The one-π and one-ρ exchange terms modified by the nuclear medium are important in describing the magnetic properties of nuclei and the nuclear spin-isospin responses. The competition between the one-pion attraction $g_\pi Q<0$ and spin-isospin repulsion $g_0'>0$, determines a degree of ''softness'' of the pionic modes in nuclei that influences directly the β-decay half-lives. So far, two basic sets of FFS parameters have been found to describe satisfactory the spin-isospin excitations in nuclei: (1) $Q=0.81$, $g'=0.9$–1.0 derived from the magnetic moments [18], which allows for a moderately soft π modes [37]; (2) $Q=0.64$, $g'=1.0$–1.1 derived from observed GT and $M1$ strength distributions [31,38,39]. A strong quenching excludes the existence of soft π modes. The recent analysis of (p,n) reaction spectra at $E_p=295$ MeV [40] and excitation energies up to $E_x<50$ MeV gives some evidences of $Q=0.93\pm0.05$, i.e., of a lower quenching than previously expected from the old (p,n) data at $E_x<30$ MeV [39]. As the experimental uncertainties are still large, both sets will be used in the calculations of the β-decay half-lives.

In a general case, the spin-isopsin $T=0$ pp effective NN interaction in Eq. (24) has a form similar to the one for $T=1$ pairing:

$$F\sigma\tau^{\xi}(\mathbf{r}_{ij})=-4N_0^{-1}(g'_{\xi}+h^{\xi}x^{q})\,\delta(\mathbf{r}_{ij}) \quad (J^{\pi}=0^{-},1^{+},\ldots), \tag{14}$$

$$F^{\xi}_{\tau}(\mathbf{r}_{ij})=-4N_0^{-1}(f'_{\xi}+h^{\xi}x^{q})\,\delta(\mathbf{r}_{ij}) \quad (J^{\pi}=0^{+},1^{-},\ldots), \tag{15}$$

where $x(\mathbf{r})$ is defined in Eq. (12). An increase of g'_{ξ} leads to shorter β^--decay half-lives and softer (p,n) spectra [longer β^+-decay half-lives and harder (n,p) spectra] [41]. This allows us to select $g'_{\xi}=0.3$–0.5 for the density-independent pairing (with $E_{\rm cutoff}=15$ MeV) from the recent (n,p) reaction data in the Fe-Co-Ni region (see Ref. [42], and references therein).

C. FFS description of the excited states in the system with pairing correlations

The CQRPA equations for the finite Fermi system with pairing correlations [18], involve the particle-hole, particle-particle, and hole-hole blocks. Assuming that the effective NN interaction is non retarded, these equations can be written in terms of the density matrix variations $\hat{\rho}_i$ in the external field $\hat{V}^0$

$$\hat{V}_i=\hat{e}_{qi}\hat{V}_i^0+\sum_k\,((\hat{F}_{ik}\hat{\rho}_{ik})), \tag{16}$$

(here the 3×3 matrix formalism of Ref. [43] is used). The density matrices are related to the effective fields by

$$\hat{\rho}_i=\sum_k\,((\hat{A}_{ik}\hat{V}_k)) \tag{17}$$

and to a linear response theory by

$$\hat{\rho}_i=\hat{\rho}_i^0+\sum_k\,((\hat{A}_{ik}\hat{F}_{ik}\hat{\rho}_k)). \tag{18}$$

In the above equations $\rho=\int(d\varepsilon/2\pi i)\hat{R}_i(\vec{r},\vec{r};\varepsilon,\omega)$, $\hat{R}_j=(\delta G,\delta F^{1,2},\delta G^h)(j=0,1,2,h)$ being the variations of the normal, anomalous, and hole Green functions in the external fields $\hat{V}_i^0$. Here and below, each pair of external brackets indicates the integration on the spatial coordinates and a summation on the total spins.

The effective field supermatrix $\hat{V}_i$ consists of the ph-vector $\hat{V}$ (a variation of the nonsingular term of the mass operator Σ in the external field $\hat{V}_0$), as well as of the pp and hh vectors $\hat{d}^{(1)}$, $\hat{d}^{(2)}$ (variations of the gaps $\Delta^{(1)},\Delta^{(2)}$). In Eqs. (16),(18) the velocity-dependent terms are not included and the effective NN-interaction $\hat{F}$ consists of the ph component F^{ω} coming from the normal part of the density functional and of the pp,hh components F^{ξ} connected to pairing energy density. Note that for a density dependent $\varepsilon_{\rm pair}$ Eq.(3), the component with $F^{\omega\xi}$ also arises, the explicit formulas are given in Refs. [41,43,44]. The operator of quasiparticle local charge $e_q[V_0]$ taking account for the (beyond the QRPA) medium renormalization of nuclear response is discussed in detail in Sec. II E.

The QRPA-propagator supermatrix $\hat{A}$ is obtained by integrating various pair products of the Green's functions over the energy variable ε. To avoid the ph basis truncation inevitable in the λ representation, Eqs. (14),(16) can be solved in the mixed (r,λ) approximation. The idea of the method is physically transparent: the nuclear pairing is important within the ''valence λ space'' only. It is defined as $\mu^{\tau}-\xi<\varepsilon<\mu^{\tau}+\xi$, where μ^{τ} are the neutron and proton chemical potentials. The corresponding part of the propagator L is constructed in the λ space and transformed to the r space. For the states far from the Fermi surface the propagator matrix degenerates into a single ph propagator $\tilde{A}$ of the system with no pairing. It is calculated via the Green functions constructed in the r space [45,46] which allows the exact inclusion of the ph continuum. Thus, the full propagator reads

$$A(\vec{r},\vec{r}';\omega)=\tilde{A}(\vec{r},\vec{r}';\omega)+\sum\,[L_{pn}(\omega)-\tilde{A}_{pn}(\omega)] \times\varphi_n^*(\vec{r}_1)\varphi_p(\vec{r}_1)\varphi_n(\vec{r}_2)\varphi_p^*(\vec{r}_2), \tag{19}$$

where the $\tilde{A}_{pn}$ term, i.e., the part of the propagator A corrected for the pairing contribution, is subtracted to avoid a double counting. The (r,λ) approximation was first developed for the non-charge-exchange case in Ref. [43], and then extended for the charge-exchange excitations in Ref. [41] (for the complete formulas including the important case of the odd-A nuclei see Ref. [44]).

D. FFS transition densities and β moments

As β decay proceeds to the discrete states $|s\rangle$ of the daughter nucleus, Eq. (17) can be replaced by the one for the transition density matrix defined as

$$\hat{\rho}_s^{\rm tr}(\omega_s)=(\hat{A}(r,r';\omega_s)\hat{g}_s(r';\omega_s)), \tag{20}$$

where the excitation amplitude $\hat{g}_s$ is a solution of the homogeneous equation

$$\hat{g}_s(\omega_s)=((\hat{F}\hat{A}\hat{g}_s(\omega_s))), \tag{21}$$

with a normalization condition [18]

$$\left(\left(\hat{g}_s^+\frac{d\hat{A}}{d\omega}\hat{g}_s\right)\right)_{\omega=\omega_s}=-1. \tag{22}$$

The beta moment for the transition $|0\rangle\rightarrow|s\rangle$ is given by

$$M_{JLS}=(2J+1)(\hat{e}_q^{JLS}\hat{V}_0^{JLS}(\vec{r})\hat{\rho}_{tr}^{JLS}(\vec{r};\omega_s)), \tag{23}$$

where the partial transition densities $\hat{\rho}_{tr}^{JLS}(\vec{r};\omega_s)$ are found from Eqs. (16),(20),(22).

For the decay to the states with $Q_\beta-\omega>S_n$, it is more convenient to use the partial β-strength functions

$$S_\beta^{JLS}(\omega,\gamma)=\frac{(2J+1)}{4\pi}(e_q^{JLS})^2\int\hat{V}_0^{JLS}(r)\hat{\rho}^{JLS}(r;\omega,\gamma)r^2dr, \tag{24}$$

where $\hat{\rho}=N\cdot{\rm Im}(\hat{A}\hat{V})$ are the density matrices Eq. (17), the explicit formulas involving their ph, pp, and hh components can be found in Ref. [44]. The transition density is normalized on the matrix element of the transition $|0\rangle\rightarrow|s\rangle$

$$|M_{os}|^2=(2J+1)|e_q^{JLS}V_0^{JLS}(r)\rho_{tr}^{JLS}(r,\omega_s)|^2$$
$$=\int_{\Delta\omega_s}S_\beta^{JLS}(\omega,\gamma)d\omega. \tag{25}$$

Here, the energy interval $\Delta\omega_s\gtrsim\Gamma_{\rm esc}+4\gamma$ includes the state $|s\rangle$ located within the β-decay window, $\Gamma_{\rm esc}$ being the corresponding escape width, and $\Gamma^\downarrow=4\gamma$ is the artificial width of the individual excitation which may be introduced in order to simplify numerical integration.

E. Reduction of the relativistic β-decay moments

In the nonrelativistic limit, the first-forbidden transitions are generated by the following external fields $\hat{V}^0=2\sqrt{\pi}V_{JLS}^0\tau^-$:

$$V_{0,1,1}^0=e_{qs}i\vec{\sigma}\cdot\vec{r}-e_{q5}\vec{\sigma}\cdot\vec{P}/2M,$$

$$V_{1,1,0}^0=\frac{1}{\sqrt{3}}(i\vec{r}-\vec{P}/2M), \tag{26}$$

$$V_{1,1,1}^0=e_{qs}\sqrt{2}[\vec{\sigma}\vec{r}]^{(1)},$$

$$V_{2,1,1}^0=e_{qs}\frac{2}{\sqrt{3}}[\vec{\sigma}\vec{r}]^{(2)}.$$

The normalization of the space-dependent external fields V_{JLS}^0 corresponds to the one accepted in Ref. [47]. The universal medium renormalization of the external fields of a different symmetry (beyond the QRPA-type correlations) is taken into account via the quasiparticle local charge operators $\hat{e}_{qi}=e_q[V_0^{JLS}]$. The so-called ''quenching factor'' $Q=e_{qs}[\sigma\tau]^2=(g_A/G_A)^2$ is usually introduced in order to suppresses the spin-isospin fields in the nuclear medium. The smaller Q, the less strength contained in the low-energy part ($\omega<\varepsilon_F$) of the spin-isospin response, and therefore the shorter the β-decay half-lives.

It was shown on the basis of the chiral symmetry and soft-pion limit that $\langle\gamma_5\rangle$ vertex is substantially amplified in the nuclear medium due to the meson-exchange currents and the effective NN interactions [48] but the details have not been well established (see Refs. [49,50]). The treatment of the response to the velocity-dependent fields $\vec{P}/2M$ and $(\vec{\sigma}\cdot\vec{P}/2M)$ is simplified if the induced fields $V=\vec{\sigma}\cdot\vec{P}/2M+V^{\vec{\sigma}\cdot\vec{P}}$ and $V'=\vec{P}/2M+V^{\vec{P}}$ are assumed to be small perturbations. These yield

$$\hat{V}^{\sigma\cdot\vec{P}}=\left(\hat{F}\hat{A}\frac{e_{q5}\vec{\sigma}\cdot\vec{P}}{2M}+\hat{F}\hat{A}\hat{V}^{\vec{\sigma}\cdot\vec{P}}\right),$$
$$\hat{V}^{\vec{P}}=\left(\hat{F}\hat{A}\frac{\vec{P}}{2M}+\hat{F}\hat{A}\hat{V}^{\vec{P}}\right). \tag{27}$$

Here F includes the velocity-dependent and spin-orbit effective interactions.

From Eqs. (16),(26),(27), it is seen that the renormalization of the spin-isospin fields is given by the FFS local charge $e_{qs}=g_A/G_A$ and (at the QRPA level) by the spin-isospin effective interactions governed by the strength parameters $g',g'_{\pi,\rho}$ of Eq. (11). The $\vec{\sigma}\cdot\vec{P}$ field is renormalized by the FFS axial local charge $e_{q5}=e_q[\gamma_5]$ and (at the QRPA level) by the one-pion exchange, spin-isospin velocity dependent (g'_1), and two-body spin-orbit (κ^-) effective NN interactions of Eqs. (4),(5). Considering only the one-pion exchange and spin-isospin velocity dependent harmonic g'_1 one arrives at $e_{q5}=(1+R)(1+\frac{2}{3}g'_1)$ [51], where the ratio of the two-particle exchange current diagram to the impulse approximation one is estimated as $0.44<R<0.62$ [49]. The FFS quasiparticle local charges used in the present calculations were $e_{q5}=1.5$ (for $g'_1=0$), $e_{q5}=1.2$ (for $g'_1=-0.4$) [51], $e_{qs}^2=0.64$ [31], and 0.81 [37]. More sophisticated formula for e_{q5} involving the Landau-Migdal tensor harmonics, as well as the one based on the chiral Lagrangian theory can be found in Ref. [50] (all the above estimates agree within 10%).

To facilitate the large-scale calculations of the first-forbidden transitions, it is convenient not to consider the relativistic β-moments explicitly. Instead, the exact relation between the relativistic vector current transition matrix element $\langle\alpha\rangle$ and its spacelike counterpart $\langle i\vec{r}\rangle$ is applied

$$\langle\alpha\rangle=\frac{\xi}{\lambda\!\!\!^{-}_e}\Lambda_1\langle i\vec{r}\rangle, \tag{28}$$

where $\lambda\!\!\!^{-}_e = 386.1$ fm is the electron Compton wavelength. The analogous approximate relation between the axial charge $\langle \gamma_5 \rangle$ and $\langle i\vec{\sigma}\cdot\vec{r}\rangle$ beta-moments can be constructed by taking into account the medium effects

$$\langle \gamma_5 \rangle = \frac{\xi}{\lambda\!\!\!^{-}_e} \Lambda_0 \langle i\vec{\sigma}\cdot\vec{r}\rangle. \tag{29}$$

The state dependent factor $\Lambda_J(i\to f;\omega)$ is found using the QRPA energy-weighted and nonweighted sum rules, the self-consistency criteria Eq. (9), and the properties of the FFS transition densities Eq. (22). Extending the approach of Ref. [31], Λ_J is represented as a sum of the irregular part and smoothed corrections

$$\xi\Lambda_J = \omega_{if} + \sum_j \overline{u}_j + \sum_k \overline{w}_k, \tag{30}$$

where $\omega_{if} = \omega - \Delta M_{np}$ is the energy of the nuclear transition satisfying the specific selection rules, ξ is the dimensionless Coulomb parameter $\xi = Ze^2/2Rm_ec^2$, Z and R being the charge and radius of the daughter nucleus, the terms on the right hand side of Eq. (30) are in units of m_ec^2.

The smoothed terms $\overline{u}_i$ originate from the Coulomb U_C, spin-orbit U_{sl}, and the symmetry U^- self-consistent potentials, while the $\overline{w}_i$ relate to the effective NN interactions F_i Eqs. (4),(5),(13). They are obtained by averaging over the neutron excess density ρ_- and spin-orbit density ρ_{sl} as follows:

$$\begin{aligned} \overline{u}_i &= e_{qs}^2 (V_0 V_0^\dagger U\rho)_i / m_0^{JLS}, \\ \overline{w}_i &= e_{qs}^2 (V_0 V_0^\dagger \rho F \rho)_i / m_0^{JLS}. \end{aligned} \tag{31}$$

Here the QRPA sum rules for the external field operators $V_0^{JLS} = e_{qs} f(r)[\sigma Y_L]^{JM}\tau_\pm$

$$\begin{aligned} m_n^{JLS} &= \sum_s \omega_s^n |\langle s|\hat{V}_0^{JLS}|0\rangle|^2 \\ &= \int d\omega [\omega^n S_{\tau_-}^{JLS}(\omega) - (-)^n \omega^n S_{\tau_+}^{JLS}(\omega)], \end{aligned} \tag{32}$$

involve the full charge-exchange strength functions for both τ_- and τ_+ channels.

For the relativistic vector β moment $\langle\alpha\rangle$, the self-consistency condition Eq. (9) provides precise cancellation of all the terms in Eq. (30), except the averaged Coulomb potential

$$\xi\Lambda_1 = \omega_{if} + \overline{u}_C. \tag{33}$$

In the case of the uniformly charged sphere $U_C = 6/5\xi$, and Eq. (33) coincides with the well-known result of Ref. [52] obtained under the CVC hypothesis.

For the axial-vector moment $\langle\gamma_5\rangle$, the sum rule estimate $\Lambda_0 = \Lambda_1$ was obtained in Ref. [52] neglecting the off-diagonal matrix element of the nuclear hamiltonian. It was used in Ref. [53] to calculate the β decays in the lead region. Within the FFS, state independent (beyond the QRPA) renormalization of the $\langle\gamma_5\rangle$ is included into the local axial charge operator e_{q5}. The renormalization of the Λ_0 associated with the effective NN interactions can be found from the FFS sum rules m_1^{011} and m_0^{011}

$$\xi\Lambda_0 = \omega_{if} + \overline{u}_C + (\overline{w}_{sl} - \overline{u}_{sl}) + (\overline{w}_{g'} - \overline{w}_{f'}) + \overline{w}_\pi. \tag{34}$$

The term $\overline{w}_{f'}$ appears here instead of $\overline{u}^-$ according to the self-consistency condition Eq. (9). The $\overline{w}_{g',\pi}$ terms correspond to the ones from Eq. (13). Once the self-consistent densities ρ^τ and spin-orbit densities ρ_{sl}^τ are found, all the terms in Eq. (34) can be evaluated.

It is instructive to estimate the different contributions to Eq. (34). The term $\overline{w}_{g'} - \overline{w}_{f'}$ coming from the spin-isospin and isospin effective NN interactions is proportional to $g' - f'$, hence it disappears in the SU(4) limit $g' \approx f'$. The remaining terms are readily evaluated if the corresponding densities ρ^-, ρ^τ, and ρ_{sl}^τ are replaced by the properly normalized Fermi type distributions. The spin-dipole non-energy-weighted sum rule is given by $m_0^{J1S} = \hat{e}_q^2[(2J+1)/2\pi](N\langle r_n^2\rangle - Z\langle r_p^2\rangle)$. The approximations $\langle r_n^2\rangle \approx \langle r_p^2\rangle$ and $\langle f|r^\lambda|i\rangle = 3R^\lambda/(\lambda+3)$ lead to $m_0^{(011)} \approx e_q^2 R^2 (N-Z)/3\pi$. The effect of the π-meson exchange (at the QRPA level) is rather small, as $\overline{w}_\pi \approx (N-Z)/2A^2$.

The major impact on Λ_0 comes from the spin-orbit effective NN interaction Eq. (4). For the $J=0$ transitions, summing the terms arising from $\overline{u}_{sl}$, and $\overline{w}_{sl}$ leads to $\overline{w}_{sl} - \overline{u}_{sl} \approx -4\langle 0|e_q^2 V_0^{(011)2}\hat{U}_{sl}|0\rangle/m_0^{(011)} = -4\Sigma_\tau (e_q^2 V_0^{(011)2} U_{sl}^\tau \rho_{sl}^\tau)/m_0^{(011)}$. Assuming $l \approx l \pm 1 \approx A^{1/3}$, and neglecting the terms to order $\sim A^{-1/3}$, the spin-orbit contribution is $(\overline{w}_{sl} - \overline{u}_{sl})/\xi \approx (8\varepsilon_F/3m_ec^2)\ \rho_0 r_0^3\ \nu(A,Z)(\kappa^+/2)A^{1/3}/(N-Z)$, where $\kappa^+ \approx 0.4$ is the isoscalar spin-orbit strength constant. The factor $\nu(A,Z)$ is introduced to take into account the number of partner levels involved and the possibility of partial occupancy of the particle level. For the highest energy transitions in $N=82$, $Z>50$ nuclei, $\Lambda_0 - \Lambda_1$ is estimated numerically to be about 20% of Λ_1.

F. The β-decay half-lives

The general expression for the partial β-decay half-life is

$$\begin{aligned} 1/t_{1/2} = D^{-1}(G_A/G_V)^2 \int_{m_ec^2}^{W_{\max}} & C_\beta(W) \\ & \times F(Z,W) p W (W_{\max} - W)^2 dW, \end{aligned} \tag{35}$$

where $C_\beta(W)$ is the β-decay shape factor, $F(Z,W)$ is the usual Fermi function with the Coulomb screening and relativistic nuclear finite size corrections taken into account [54], $D = 6163 \pm 4$ s, W is the electron energy, and $W_{\max} = W_0 + m_ec^2$ is the total disintegration energy. The shape factor is given by the exact expression

$$C_\beta(W) = \frac{\sum_{k_e, k_{\bar{\nu}}, J} C_J(k_e, k_{\bar{\nu}})}{F(Z,W)(W_{\max} - W)^2 p^2}, \tag{36}$$

where $J=|k_e-k_\nu^{\rightarrow}|$ is the momentum transferred to the lepton pair, and the coefficients $C_J(k_e,k_\nu^{\rightarrow})$ are the standard combinations of β moments and leptons wave functions at the nuclear radius [55].

For the nonunique forbidden decays with $E_{\rm Coul}\gg\omega$, the distortion of the electron spectra is not significant and the shape factor is energy independent

$$C_\beta=\frac{\xi}{\chi_e}\sum_{J=0,1}B(J)=\sum_{J=0,1}\left|\frac{\sum_{S=0,1}\langle f|M_{JLS}|i\rangle}{2J+1}\right|^2, \quad (37)$$

which is called the Coulomb (ξ) approximation. The orbital β-decay term with $J=2$ does not contain ξ and can be neglected.

The total half-lives can be calculated within the β-strength function formalism

$$1/T_{1/2}=D^{-1}(G_A/G_V)^2\int_0^{Q_\beta}d\omega f_0(Z,\omega)\sum_{n=1,4}\langle\kappa_J\rangle S_n(\omega,\gamma), \quad (38)$$

where the sum contains the GT term with $J=1$ and the first-forbidden terms with $J=0,1,2$. For the GT and nonunique first-forbidden decays $\langle\kappa_{J=0,1}\rangle=1$, and for the unique first-forbidden decays, $\langle\kappa_{J=2}\rangle=f_1/f_0$, with f_1 calculated as in Ref. [56]. The integrated lepton $(e^-,\overline{\nu_e})$ phase-space volume

$$f_0=\int_{m_ec^2}^{W_{\rm max}}F(Z,W)pW(W_{\rm max}-W)^2dW \quad (39)$$

incorporates the Coulomb and finite-size corrections [54].

III. THE β-DECAY HALF-LIVES NEAR $N=50,82,126$ NEUTRON CLOSED SHELLS

A. β decay in the $Z=28$, $N=50$ region

According to available experimental [24–26] and predicted [16,20] decay schemes, the nuclei in the vicinity of $Z=28$, $N=50$ shell sequence undergo fast high–energy GT decays which are built mainly on the simple shell-model configurations $\nu 1f_{7/2,5/2}\rightarrow\pi 1f_{7/2,5/2}$ and $\nu 1g_{9/2}\rightarrow\pi 1g_{9/2}$. It is of importance that the high–energy GT transitions exist both at $Z<28$ and at $Z=28$–29 when the $\pi 1f_{7/2}$ orbital is completely blocked. The first-forbidden decays are due mainly to the $\nu 1g_{9/2}\rightarrow\pi 1f_{7/2}$ and $\nu 1f_{5/2}\rightarrow\pi 1d_{5/2}$ transitions with the energies close to that of the GT decays. In Fig. 1 we show our predictions for Ni isotopes obtained including the first-forbidden decays. Two different ground state descriptions are used, the DF3- and MSk7-based calculations (Fig. 1) being in better agreement with the experimental data than our previous ETFSI results [20]. Note that this improvement results in part from the reduction of the half-lives caused by the stronger effective pp interaction used in the present calculations.

For $Q=0.81$, the half-lives are roughly 20% shorter than for $Q=0.64$ (Fig. 1) due to the corresponding increase of the strength in the Q_β window. For the β decays in $Z\approx 28$, $N=50$ region, momenta transfer are small, and a ''softening'' of the GT strength function due to the one-π-exchange is not significant. Forbidden decays are more sensitive to the momentum dependence of the NN interaction caused by the one-π and one-ρ exchange.

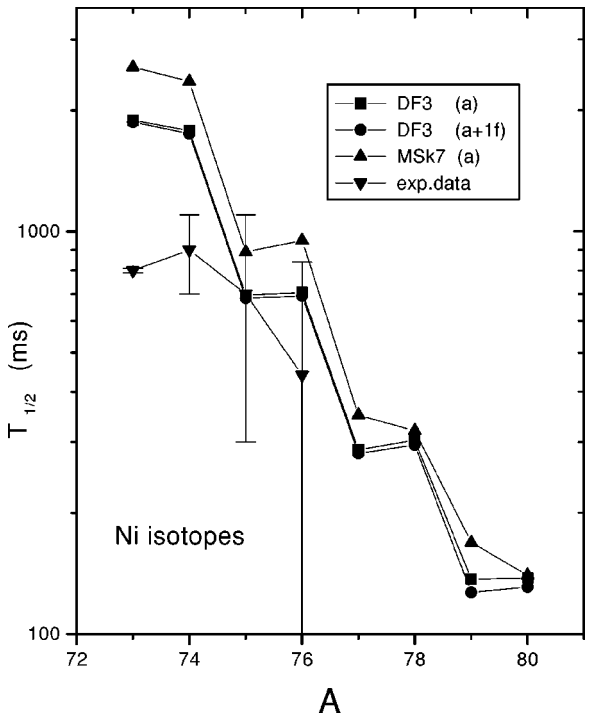

FIG. 1. The experimental β-decay half-lives for the Ni isotopes taken from Ref. [24] and NUBASE compilation [57] compared to the MSk7 and DF3 calculations ($Q=0.81$, a: allowed transitions, $a+1f$: allowed and first-forbidden transitions).

We see from Fig.1 that approaching the $N=50$ closed shell, the MSk7 half-lives agree well with the DF3 ones and existing experimental data. At smaller neutron numbers (^{73,74}Ni), the deviations are more pronounced. This can be related to the different pairing force parameters in the MSk7 [33] and DF3. (In the present paper we discuss the calculations with the density-independent pairing only.) Importantly, it may also indicate that the constraint of a better mass fit imposed on the MSk7 could distort the balance between the mean-field and pairing potentials, thus modifying the quasiparticle energies important for the half-life predictions. As the higher order corrections to the BCS are ignored, the particle number nonconservation effects may also affect the half-lives.

The first-forbidden transitions are of little effect for nuclei near $Z=28$, $N=50$ (Fig. 1). In this region, our calculations predict a number of GT and first-forbidden transitions with comparable energies, hence the GT decay channel dominates. Note that this picture does not change in the $Z=28,29$ nuclei in which the important $\pi 1f_{7/2}$ orbital is fully blocked, while many high-energy GT transitions remain open.

B. β decay in the $Z=50$, $N=82$ region

In the $1p1h$ approximation, the only high-energy GT transition in these nuclei corresponds to the $\nu 1g_{7/2}$

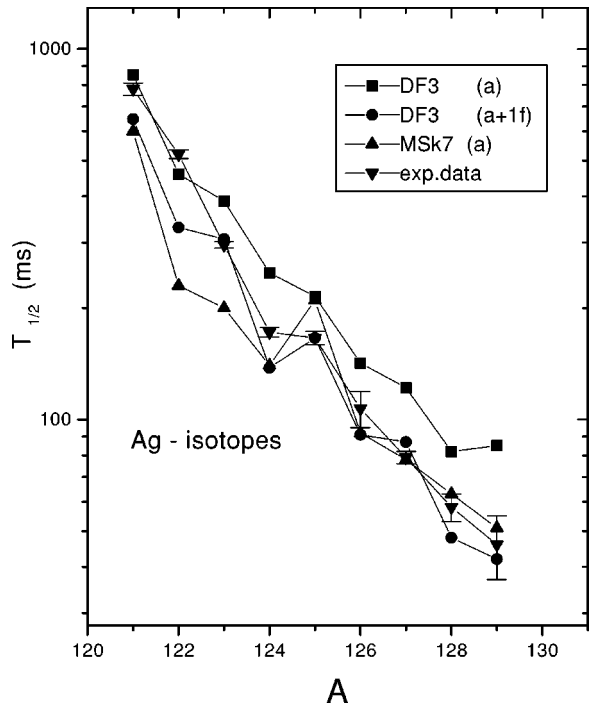

FIG. 2. The experimental β-decay half-lives for the Ag isotopic chain taken from the NUBASE compilation [57] and RILIS CERN data [25,26] compared to the predictions based on the DF3 and Msk7 ($Q=0.81$, a: allowed transitions, $a+1f$: the first-forbidden transition included).

$\rightarrow \pi 1g_{9/2}$ configuration, and the high-energy first-forbidden decay is mainly due to the $\nu 1h_{11/2} \rightarrow \pi 1g_{9/2}$ configuration. It is of interest to compare the DF3 and MSk7 calculations for the allowed GT β decays. One observes from Fig. 2 that MSk7 predicts much shorter half-lives than DF3 does for the Ag isotopes. As in the case of the Ni isotopes, the agreement between the calculations based on these models for the ground states gets worse when moving away from the $N=82$ closed shell. The calculations show that the first-forbidden transitions have a moderate impact on the total half-lives for nuclei near $Z<50$, $N=82$. For the Ag and Cd isotopes (Figs. 2,3), the first-forbidden transitions are responsible for up to a factor of 2 reduction in the total half-lives. A slight odd-even effect in the total half-lives is observed in the experimental data and in our calculations for Ag,Cd isotopes (Figs. 2,3). It is due to the odd-even staggering of the corresponding transition energies. The results for the Ag and Cd nuclei support the conclusion that the high energy GT decays dominate the total half-lives of the nuclei in the $Z<50$ region near ^{132}Sn [17,20]. Unlike in the $Z=28$ region, the high-energy GT and first-forbidden β transitions mentioned above are no longer possible, for $Z=50$-51 nuclei above ^{132}Sn, as the $1\pi g_{9/2}$ orbital is fully blocked. Due to the phase space effect, the higher energy forbidden transitions related to the $\nu 2f_{7/2} \rightarrow \pi 1g_{7/2}$, $\nu f_{7/2} \rightarrow \pi 2d_{5/2}$ configurations dominate the total half-life. For nuclei with $Z \geqslant 52$ and $N \approx 82$, $1\pi g_{9/2}$orbital is deblocked due to pairing correlations, and the GT transition strength is quenched by the occupancy factor of the proton level $(1-v^2_{1\pi g_{9/2}})$.

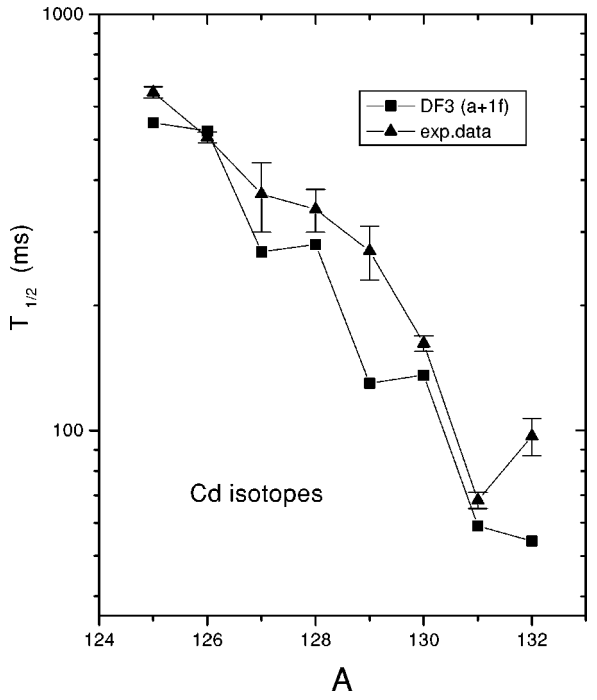

FIG. 3. The same as Fig. 2 for the Cd isotopes. The experimental data are from the NUBASE [57] and Ref. [58].

For the $^{133-139}$Sn isotopes, the FRDM calculations [16] performed in the allowed transition approximation strongly overestimate the experimental half-lives (Fig. 4). A fairly good agreement of our calculations with the experiment (Fig.

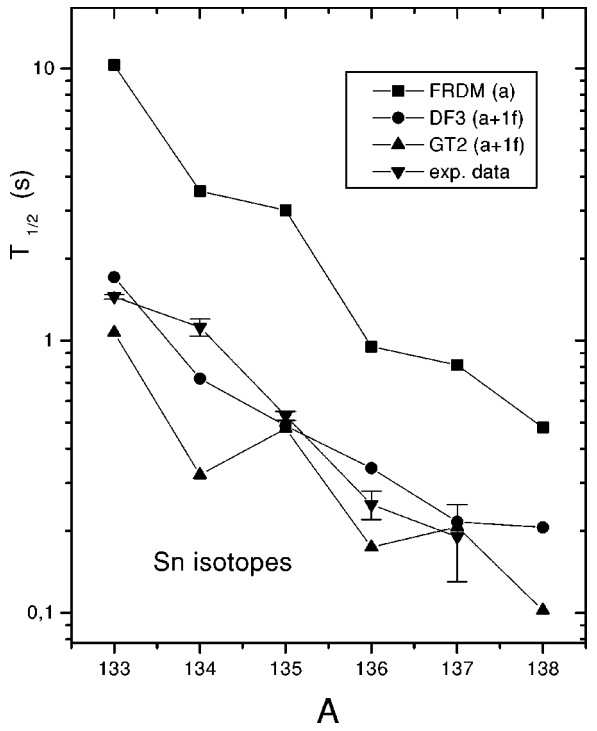

FIG. 4. The same as Fig. 2 for the Sn isotopes. The experimental data are from Ref. [26].

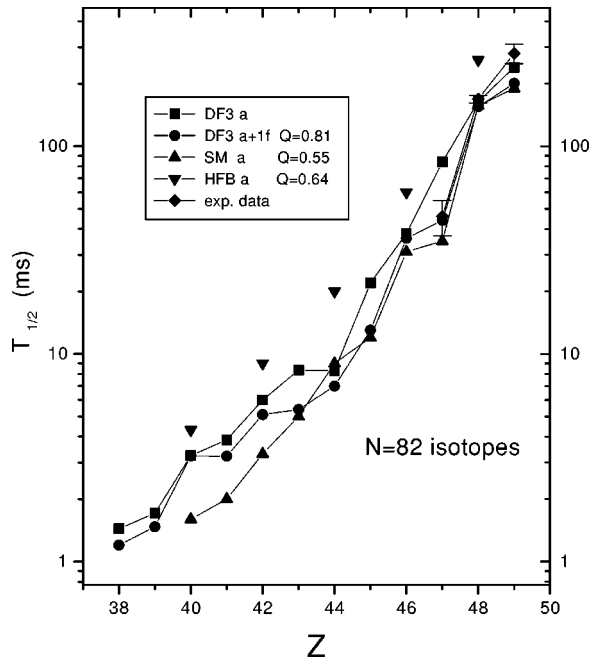

FIG. 5. The experimental β-decay half-lives for the $N=82$ chain taken from the NUBASE compilation [57] compared to DF3 ($Q=0.81$, a: allowed transitions, $a+1f$: the first-forbidden transition included), HFB [22] ($Q=0.64$) and shell-model results [3] ($Q=0.55$).

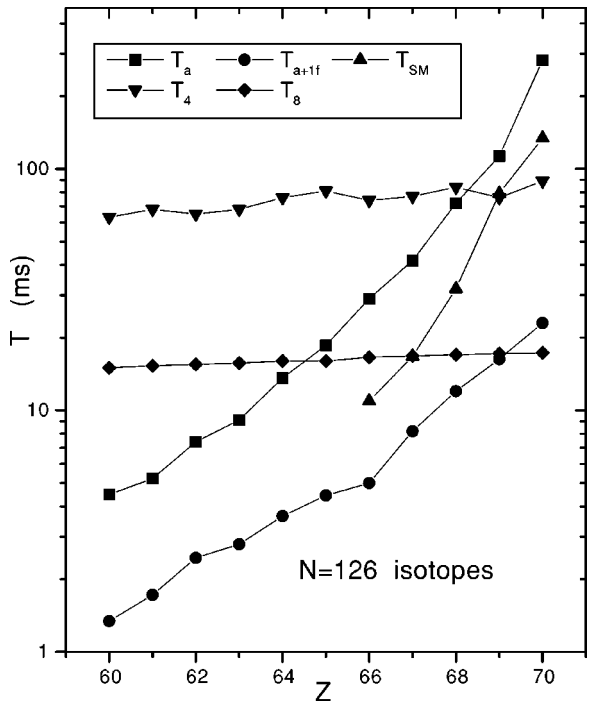

FIG. 6. The β-decay half-lives for the $N=126$ chain calculated with the DF3 ($Q=0.81$, a: allowed transitions, $a+1f$: the first-forbidden transition included) and with the shell-model [4] (T_{SM}, $Q=0.55$ was used). Also shown are the half-lives against the (ν_e,e^-) capture at the electron neutrino temperatures $T_\nu=4$ MeV (T_4) [20] and 8 MeV (T_8) [60] calculated for $L_\nu=10^{52}$ erg s^{-1} and $R=100$ km.

4) shows that Coulomb decay mechanism dominates in these nuclei. The experimental evidence of the high-energy first-forbidden transitions above ^{132}Sn has long been known [59].

In the recent study [26], the β-decay half-lives have been measured up to ^{138}Sn. Within the Q_β window of 9.0 MeV, the experimental decay scheme for ^{135}Sn demonstrates the existence of low energy GT transitions at 4–5 MeV and of high energy first-forbidden transitions at 7–9 MeV [26]. The total half-lives of 450(50) ms and 520(30) ms have been reported in Ref. [26] for ^{135}Sn in agreement with 0.6(0.1) s found earlier in Ref. [59]. Our estimate [23] was 2470 ms for the pure GT decay and 520 ms with first-forbidden decays included. The present calculations give the half-life of 482 ms for ^{135}Sn.

In Fig. 5 we display the results of the DF3 calculations ($Q=0.81$) of pure GT decays and including the first-forbidden decays for nuclei at $N=82$ and $Z<50$. The comparison is made with the HFB results [22] obtained with the same particle-particle interaction strength g'_ξ as in the present work and $Q=0.64$. Also shown are the shell-model results [3] and measured half-lives. Our calculations including the first-forbidden decays show a small odd-even effect which is in agreement with available experimental data. Note that the use of the same quenching $Q=0.81$ would drive the HFB results in closer agreement with our results and the experimental data. For the shell-model calculations [3], reducing the quenching would drive the results below the experimental data. It is worth to mention that for tin isotopes the existence of the next magic shell-closure at $Z=50$, $N=126$ is not overruled. Our DF3-based calculations give the ^{174}Sn to be the last bound tin isotopes, it turns to be ^{170}Sn within the MSk7. At the same time, the energy-dependent T-matrix interaction leads to the neutron drip-line located above ^{200}Sn [36]. With the ''modified'' neutron drip-line a role of forbidden decays may be more important, as the driving operators contain the factor r/R_0. A possible existence of superallowed Fermi, as well as accelerated Gamow-Teller and first-forbidden β decays may be anticipated in doubly-magic drip-line systems. Our RPA estimate of the half-life for ^{174}Sn is 0.58 ms for the pure GT decay and 0.18 ms with the first forbidden decays included. This subject deserves a further study.

C. β decay vs (ν_e,e^-) capture in $N=126$ region

In the important r-process region near $Z\approx 60$–75 and $N=126$, the role of the first-forbidden decays is decisive. These nuclei undergo high-energy first-forbidden decays related to the $\nu 1i_{13/2}\rightarrow\pi 1h_{11/2}$ configuration. Our CQRPA calculations predict a strong $J^\pi=1^-(S=1)$ transitions in nuclei near $Z\approx 70$ and $N=126$. Their β-decay energies are of about 6 MeV, well above the GT transitions at about 4 MeV which are related to the $\nu 1h_{9/2}\rightarrow\pi 1h_{11/2}$ configuration weakened due to the partial occupancy of the $1h_{11/2}$ level. The unperturbed β-decay energy of the main GT decay configuration $\nu 1i_{13/2}\rightarrow\pi 1i_{11/2}$ is low (about 1 MeV). Thus, it is clearly

seen from Fig. 6. that the behavior of the half-lives for the GT and GT+first-forbidden transitions reflects the blocking of the $1\pi g9/2$ and $1\pi h11/2$ levels with increasing Z.

In Fig. 6 a comparison is presented with the shell-model calculations [3] performed in the allowed transition approximation and with $Q=0.55$. It is seen that the inclusion of the first-forbidden transitions results in noticeably shorter half-lives in the $N=126$ region. The difference with the GT approximation amounts to typically a factor 5 to 10, and is more pronounced for heavier nuclei approaching the closed proton shell at $Z=82$. Note that the shell-model half-lives of Ref. [4] would be shorter if the first-forbidden decays were included and/or a smaller quenching used.

The shorter half-lives predicted for $N=126$ should have significant implications on the r-process nucleosynthesis in this region. In the specific case of the neutrino wind model [2], the charged-current electron neutrino captures by heavy nuclei (ν_e,e^-) can compete with the β decays in driving the material to higher Z elements. Thus, the effective ''weak flow'' rate is given by $\lambda_{\rm eff}=\lambda_\beta+\lambda_\nu$. The neutrino capture rates are, however, sensitive to the adopted neutrino driven wind model, since they depend on the neutrino flux which scales with the R^2—the distance to the center of the neutron star. The (ν_e,e^-)-capture rates would also increase if the neutrino oscillations $\nu_e \rightleftharpoons \nu_{\mu,\tau}$ are included. We show in Fig. 6 the calculated half-lives against the (ν_e,e^-) capture [20] corrected for the contribution of forbidden transitions at the electron neutrino temperature $T_\nu=4$ MeV, and also the calculations by Ref. [60] at $T_\nu=8$ MeV (for this temperature the complete neutrino oscillations were assumed in Ref. [60]). In both calculations the neutrino energy luminosity $L_\nu=10^{52}$ erg s^{-1} and $R=100$ km are used.

One observes from Fig. 6 that for nuclides with $Z\leqslant 69$ our calculated β-decay rates are higher even than the (ν_e,e^-) rates at $T_\nu=8$ MeV with the neutrino oscillations included [60]. In other words, for these given temperatures and neutrino flux, β decays dominate over charged-current electron neutrino captures. The impact of the present calculations on speeding up the r-process nucleosynthesis remains to be studied.

D. β decay in the region "east" of ^{208}Pb

The possibilities of experimental measurements near $N=126$ are very limited. The current experiments (see [28,46]) concern mostly the nuclei ''east'' and ''west'' of ^{208}Pb. In the region close to ^{208}Pb, the strong first-forbidden β decays are well known experimentally. Numerous theoretical studies [53,61,62] have shown a complicated character of the first-forbidden decays near ^{208}Pb, with their relatively low Q_β values and transition energies. The main problem the models encounter lies in a near cancellation of the leading matrix elements for $J=0,1$ transitions which results in a deviation of the electron spectra from a statistical shape. In this case, the ξ approximation may fail, and the Behrens-Bühring multipole expansion of the β-spectrum form factors [30] is needed. While a detailed analysis of the β decays in the ^{208}Pb region requires due consideration of the energy dependence of the shape factor, further to the ''east'' of ^{208}Pb, a simple estimate the total half-lives within the Coulomb (ξ) approximation is of interest. The main aim is to study the accuracy and limitations of the present model for large-scale calculations. Figures 7–9 show the calculated half-lives for the $^{209-214}$Tl, $^{215-218}$Pb, and $^{215-220}$Bi isotopes where the

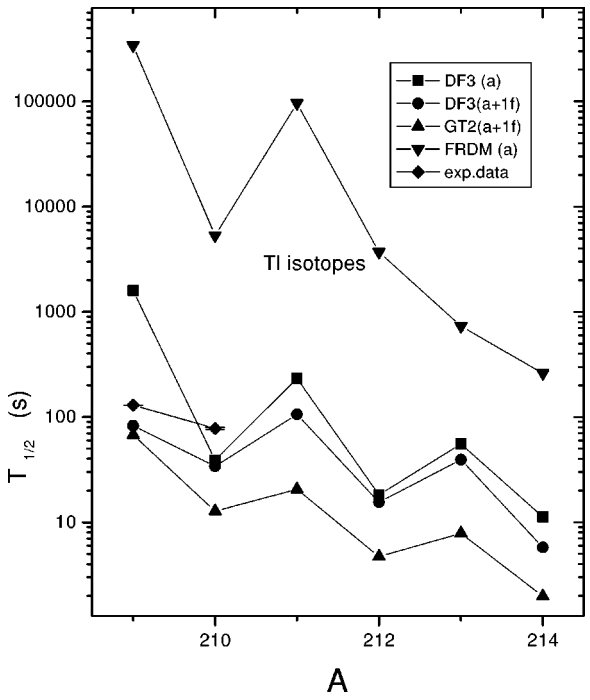

FIG. 7. The β−decay half-lives for Tl isotopes calculated within the DF3+cQRPA ($Q=0.81$, a: allowed transitions, $a+1f$: the first-forbidden transition included) FRDM and GT2 models [16,14]. The experimental half-lives are taken from NUBASE [57] and [27].

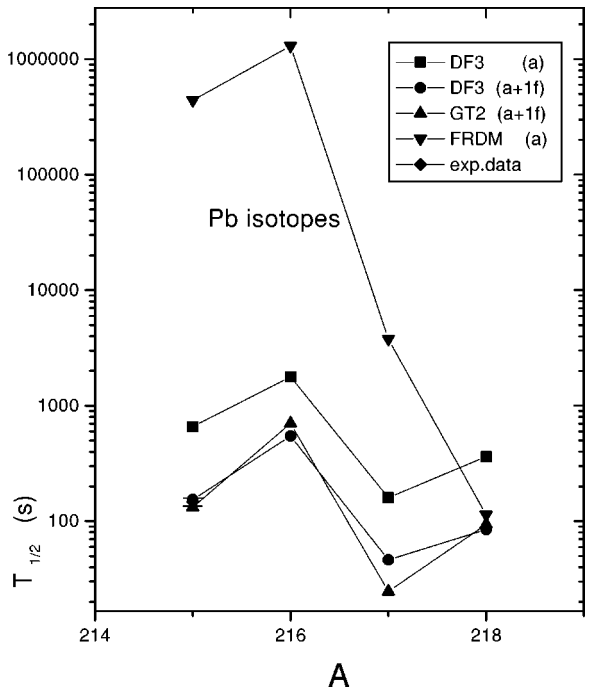

FIG. 8. The same as Fig. 7 for Pb isotopes. The experimental data are from Ref. [28].

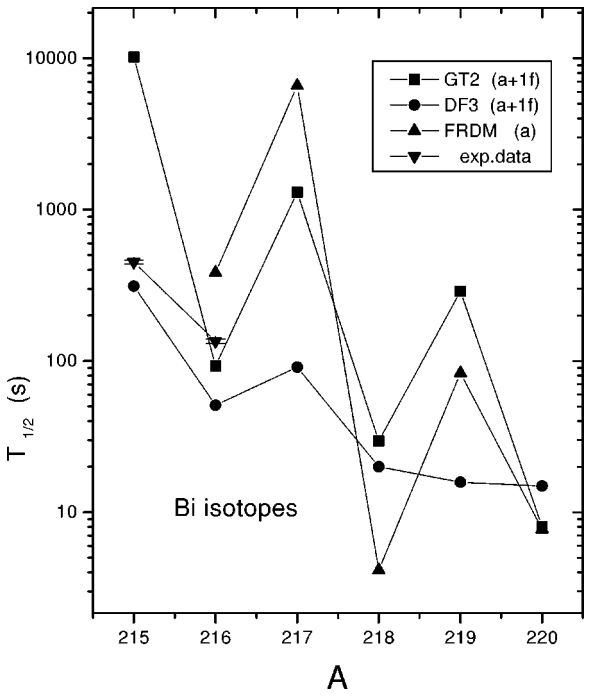

FIG. 9. The same as Fig. 7 for Bi isotopes. The experimental data are from the NUBASE [57].

calculated Q_β values are relatively high and varyin the intervals of 3.1–6.4, 2.1–2.2 and 2.8–5.7 MeV, respectively.

The half-lives based on FRDM [16] and on the semistatistical version of ''gross-theory'' GT2 [14] are also presented. Figures 7–9 indicate that the FRDM calculations using the GT transition approximation [16] overestimate the available experimental data by orders of magnitude. Our β-decay half-lives calculated for these nuclei in the GT approximation are much shorter than the FRDM ones. This is because of the different treatment of the ground state properties and pairing correlations, and also due to the pp effective interaction not included in Ref. [16].

The results of global GT2 calculations [14] with a parametric description of the forbidden transitions, vary significantly from one isotopic chain to the other (Figs. 7–9). For example, the extent of the odd-even effects in the Tl isotopes (Fig. 7) predicted by the GT2 and FRDM calculations, has been not confirmed by recent experimental data [28]. For these isotopes, our calculations show an important contribution of the GT transitions to the total half-lives. According to the ground state and pairing properties predicted by DF3, the GT strength can come from the stretched $(\nu 1i_{11/2}\pi 1i_{13/2})$ quasiparticle configuration with the partially occupied $\nu 1i_{13/2}$ level. The major first-forbidden strength in the Tl, Pb and Bi isotopes is related to the $(\nu 1g_{9/2}\pi 1h_{9/2})$, $(\nu 1g_{9/2}\pi 1f_{7/2})$, as well as to partially blocked $(\nu 1k_{15/2}\pi 1i_{13/2})$ shell-model configurations.

Even though our calculations show a fairly regular behavior of the total half-lives (Figs. 7–9), they may be oversimplified in the specific region ''east'' of ^{208}Pb. Their accuracy may decrease, for example, when the $\Delta J=0$ transitions dominate in the decay schemes. This is mainly due to the neglect of the velocity-dependent terms in the effective NN interaction and to the use of the Coulomb (ξ) approximation. However, in general, the results are in a qualitative agreement with available experimental data on total half-lives. Thus, they may provide a useful guide for the planning of the new experiments in this region of the nuclear chart.

IV. CONCLUSIONS

The developed density functional+CQRPA approach is based on the self-consistent description of the ground state properties and imposes no restriction on the ph single-particle basis. This allows us to derive the mass-independent (finite-range ph and pp) effective NN interactions of FFS and the energy independent spin-isospin local charge $Q=e_{qs}^2$ from experimental data on the spin-isospin responses of nuclei (with no direct fitting to the β-decay half-lives).

A special feature of the method is that the space-dependent operators of the first-forbidden decay are treated implicitly, while the relativistic β moments $\langle\alpha\rangle$ and $\langle\gamma_5\rangle$ are reduced to their space-dependent counterparts. An approximation based on the self-consistent FFS sum rules takes into account the renormalization of the $\langle\gamma_5\rangle$ in nuclear medium. The comparison with the newly measured experimental half-lives shows that the method provides a reasonably accurate prediction of the total half-lives important for the r process. This gives some confidence that the model developed here provides a framework for microscopic global calculations of the Gamow-Teller and first-forbidden decays for the r-process relevant nuclei.

The calculations of the total half-lives for nuclei near the $N=50,82$ closed shells show a better agreement with available experimental data than our previous ETFSI results [20]. For these nuclei crucial for the r-process modeling, the high energy GT decays dominate the total half-lives. The effect of first-forbidden transitions is found to be small for $N=50$ region, and moderate for $N=82$ region. In contrast, the effect of the high-energy first-forbidden transitions is found to be decisive in the $Z\geqslant 50$, $N\approx 82$ and especially in the $N=126$ regions. The impact of the improved half-lives on the r-process abundances will be analyzed in the forthcoming paper.

We have performed the calculations of the total half-lives in the regions where high-energy GT and first-forbidden decays dominate. For the nuclei in which a retardation of the forbidden decays plays a role, due to the specific selection rules, nuclear deformation effects, a cancellation of the competing β moments, etc. [30], the approximations used above may be too simplistic. To properly describe these features (especially for partial half-lives), an extension of the method will be needed. An advanced framework for the universal description of the first-forbidden transitions requires a refined treatment the electron radial wave functions [30]. An implicit treatment of the $\langle\alpha\rangle$ and $\langle\gamma_5\rangle$ β moments is also needed along with the inclusion of the velocity-dependent and spin-orbit terms to the effective NN interaction.

ACKNOWLEDGMENTS

The author would like to thank the Institute for Nuclear Theory at the University of Washington for warm hospitality and the U.S. Department of Energy for partial support during the completion of this work. Support within the ISSN grant of the FNRS, Belgium is gratefully acknowledged. It is a pleasure to thank M. Arnould for continuous interest in this work, W. C. Haxton and G. F. Bertsch for stimulating discussions. I am grateful to S. V. Tolokonnikov for valuable advices improving the paper and to the participants of the Program IAP P5/07 ''Exotic nuclei for Nuclear Physics and Astrophysics'' at the IKS, Leuven for numerous discussions.

[1] Y.-Z. Qian and S.E. Woosley, Astrophys. J. **471**, 331 (1996).
[2] G. McLaughlin and G. Fuller, Astrophys. J. **489**, 766 (2000).
[3] G. Martinez-Pinedo and K. Langanke, Phys. Rev. Lett. **83**, 4502 (1999).
[4] G. Martinez-Pinedo, Nucl. Phys. **A668**, 357c (2000).
[5] E. Caurier, P. Navratil, W.E. Ormand, and J.P. Vary, Phys. Rev. C **66**, 024314 (2002).
[6] E.K. Warburton, Phys. Rev. C **C44**, 233 (1991); E.K. Warburton and I.S. Towner, Phys. Lett. B **294**, 1 (1992).
[7] N. Michel, J. Okolowicz, F. Nowacki, and M. Ploszajczak Nucl. Phys. **A703**, 202 (2002).
[8] J. Dukelsky *et al.*, Phys. Rev. **65**, 054309 (2002).
[9] L. Zamic *et al.* Phys. Rev. **65**, 054314 (2002).
[10] A.V. Smirnov, S.V. Tolokonnikov, and S.A. Fayans, Sov. J. Nucl. Phys. **48**, 995 (1988); S.A. Fayans, S.V. Tolokonnikov, E.L. Trykov, and D. Zawischa, Nucl. Phys. **A676**, 49 (2000).
[11] J. Meng and P. Ring, Phys. Rev. Lett. **77**, 3963 (1996).
[12] M. Matsuo, Nucl. Phys. **A696**, 371 (2001).
[13] A. Bulgac, Phys. Rev. C **65**, 051305(R) (2002).
[14] T. Tachibana, M. Yamada, and N. Yoshida, Prog. Theor. Phys. **84**, 641 (1992).
[15] M. Hirsch, A. Staudt, and H-V. Klapdor-Kleingrothaus, At. Data Nucl. Data Tables **51**, 244 (1992); M. Homma *et al.*, Phys. Rev. C **54**, 2972 (1999).
[16] P. Möller, J.R. Nix, and K.-L. Kratz, At. Data Nucl. Data Tables **66**, 131 (1997).
[17] I.N. Borzov, S.A. Fayans, E. Kromer, and D. Zawischa, Z. Phys. A **355**, 117 (1996).
[18] A.B. Migdal, *Theory of Finite Fermi Systems and Atomic Nuclei Properties* (Interscience, New York, 1965).
[19] I.N. Borzov, S. Goriely, and J.M Pearson Nucl. Phys. **A621**, 307c (1997); www-astro.ulb.ac.be
[20] I.N. Borzov and S. Goriely, Phys. Rev. C **62**, 035501 (2000).
[21] S. Goriely, M. Arnould, I.N. Borzov, and M. Rayet, Astron. Astrophys. **375**, 35L (2001).
[22] M. Bender, J. Dobaczewski, W. Nazarewicz, R. Surman, and J. Engel, Phys. Rev. C **60**, 014302 (1999).
[23] I. N. Borzov, in *Proceedings of the NATO Advanced Research Workshop on Nuclear Many Body Problem 2001*, Brijuni, Pula, Croatia, edited by W. Nazarewicz and D. Vretenar (Kluwer, Dordrecht, 2002), p. 323
[24] S. Franchoo *et al.*, Phys. Rev. Lett. **81**, 3100 (1998).
[25] V.N. Fedoseev *et al.*, Z. Phys. A **353**, 9 (1995).
[26] J. Shergur *et al.*, Nucl. Phys. **A682**, 493c (2001); Phys. Rev. C **65**, 034313 (2002).
[27] J. Kurpeta *et al.*, Eur. Phys. J. A **7**, 49 (2000).
[28] H. De Witte (private communication).
[29] S.A. Fayans and V.A. Khodel, Zh. Eksp. Teor. Fiz. **17**, 633 (1970).
[30] H. Behrens and W. Bühring, *Electron Radial Wave Functions and Nuclear Beta-decay* (Clarendon, Oxford, 1982).
[31] N.I. Pyatov and S.A. Fayans, Sov. J. Part. Nucl. **14**, 401 (1983).
[32] K.A. Mezilev *et al.*, Phys. Scr. **T56**, 227 (1995).
[33] S. Goriely, F. Tondeur, and J.M. Pearson, At. Data Nucl. Data Tables **77**, 311 (2001).
[34] G. Audi and A.H. Wapstra, Nucl. Phys. **A624**, 1 (1997).
[35] J. Dobaczewski *et al.*, Phys. Rev. C **53**, 2809 (1996).
[36] M. Baldo, U. Lomardo, E.E. Saperstein, and M. Zverev Phys. Lett. B **533**, 17 (2002).
[37] I.N. Borzov, E.E. Saperstein, S.V. Tolokonnikov, and S.A. Fayans, Sov. J. Part. Nucl. **12**, 848 (1981).
[38] I.N Borzov, S.V. Tolokonnikov, and S.A. Fayans, Sov. J. Nucl. Phys. **40**, 732 (1984).
[39] C. Gaarde, Nucl. Phys. **A396**, 127 (1983).
[40] T. Wakasa *et al.*, Phys. Rev. C **55**, 2909 (1999).
[41] I.N. Borzov and E.L. Trykov, Yad. Fiz. 52, 52 (1990) [Sov. J. Nucl. Phys. **52**, 33 (1990)]; I.N. Borzov, E.L. Trykov, and S.A. Fayans, *ibid.* **52**, 627 (1990).
[42] A.L. Williams *et al.*, Phys. Rev. C **51**, 1144 (1995).
[43] A.P. Platonov and E.E. Saperstein, Nucl. Phys. **A486**, 118 (1988).
[44] I.N. Borzov, S.A. Fayans, and E.L. Trykov, Nucl. Phys. **A584**, 335 (1995).
[45] S. Shlomo and G. Bertsch, Nucl. Phys. **243**, 507 (1975); G. Bertsch and S.F. Tsai, Phys. Rep. **18**, 126 (1975).
[46] E.E. Saperstein, S.V. Tolokonnikov, and S.A Fayans, Report No. IAE-2570, 1975; I.N. Borzov and S.A Fayans, Report No. FEI-1129, 1980.
[47] A. Bohr and B. Mottelson *Nuclear Structure* (Benjamin, New York, 1969), Vol. I.
[48] K. Kubodera, J. Delorme, and M. Rho, Phys. Rev. Lett. **40**, 755 (1978).
[49] M. Rho and G.E. Brown, Comments Nucl. Part. Phys. **10**, 201 (1981).
[50] C. Song, Phys. Rep. **347**, 289 (2001).
[51] R.U. Khafizov and S.V. Tolokonnikov, Phys. Lett. **153B**, 353 (1985); **162B**, 21 (1985).
[52] T. Ahrens and E. Feenberg, Phys. Rev. **86**, 64 (1952).
[53] F. Krmpotic, K. Ebert, and W. Wild, Nucl. Phys. **A342**, 497 (1980).
[54] N.B Gove and M.J. Matrin, At. Data Nucl. Data Tables **10**, 206 (1971).
[55] H.E. Bosch *et al.*, Phys. Rev. C **7**, 760 (1973).
[56] L.N. Zyranova, *Unique Beta Transitions* (Academy of Science USSR, Moscow, 1960); *Once Forbidden Beta Transitions* (Pergamon, Oxford, 1963).

[57] G. Audi and A.H. Wapstra, Nucl. Phys. **A624**, 1 (1997).
[58] M. Hannawald *et al.*, Phys. Rev. C **62**, 054301 (2000).
[59] J. Blomquist, A. Kerek, and B. Fogelberg, Z. Phys. A **314**, 199 (1983).
[60] A. Hektor, E. Kolbe, K. Langanke, and J. Toivanen, Phys. Rev. **61**, 055803 (2000).
[61] S.A. Fayans and V.A. Khodel, Phys. Lett. **30B**, 5 (1969).
[62] I.S. Towner, Phys. Rep. **155**, 263 (1987).